

High-resolution optical interferometry from the modelling point of view

· 1"

Observing techniques, instrumentation and science for metre-class telescopes III

M. Brož, P. Harmanec, D. Mourard, J. Budaj, ...

Interferometric instruments

• CHARA/VEGA	$B/\lambda = 6 \cdot 10^8$ c. per b.	Mourard et al. (2009)
• CHARA/MIRC-X	2.7	Anugu et al. (2020)
• CHARA/MYSTIC	1.5	Setterholm et al. (2023)
• CHARA/SPICA	5.1	Mourard et al. (2018)
• VLTI/AMBER	1	Petrov et al. (2007)
• VLTI/PIONIER	0.7	LeBouquin et al. (2011)
• VLTI/GRAVITY	0.5	Abuter et al. (2018)
• VLTI/MATISSE	0.3	Lopez et al. (2022)
• NPOI	7.9	Armstrong et al. (2013)
• LBTI	0.1	Hinz et al. (2016)
• ALMA	0.5	Wootten et al. (2009)
• EHT, ...	50	Akiyama et al. (2019)

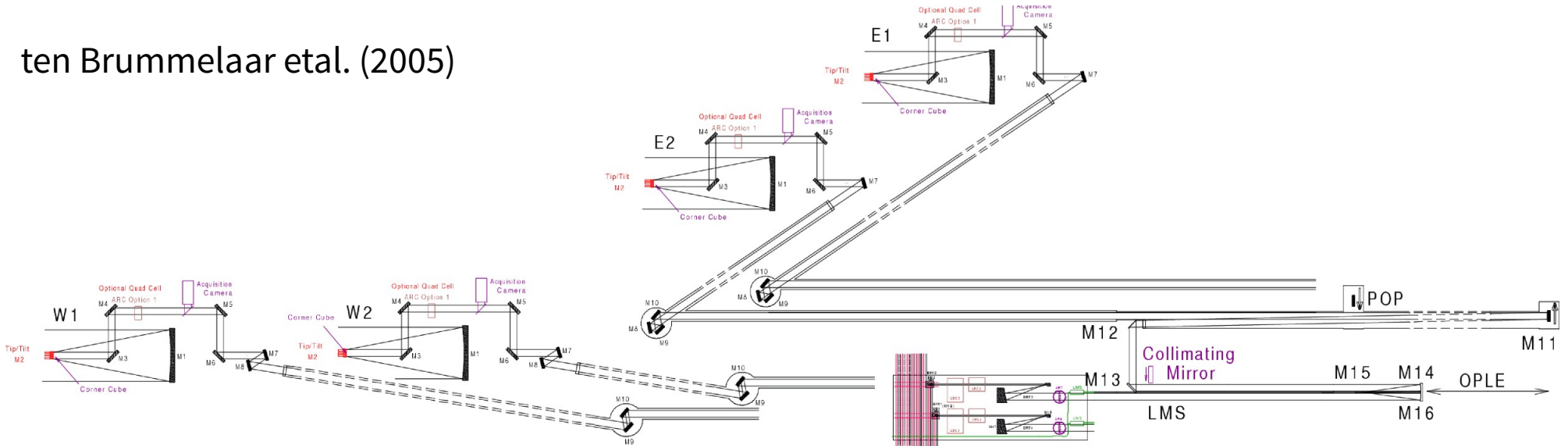
CHARA

- Mt. Wilson, 6 telescopes, 1-m, Mersenne afocal, Y arrangement
- 10 baselines up to 331 m, $B/\lambda = 331 \text{ m}/550 \text{ nm} = 6 \cdot 10^8$ cycles per baseline



ten Brummelaar et al. (2005)





Mersenne telescope

- Nasmyth
- coudé
- rotating box
- fixed delay
- periscope
- delay line
- 2nd Mersenne telescope
- dichroic mirrors V/IR

Beams

Visible Imager

Tip/Tilt

Fringe Tracking

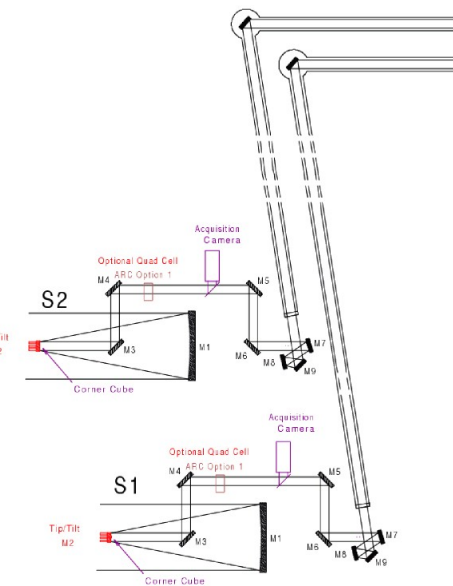
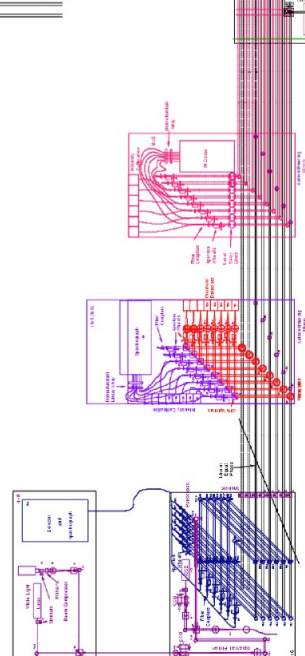
Alignment

IR Imager

Optional

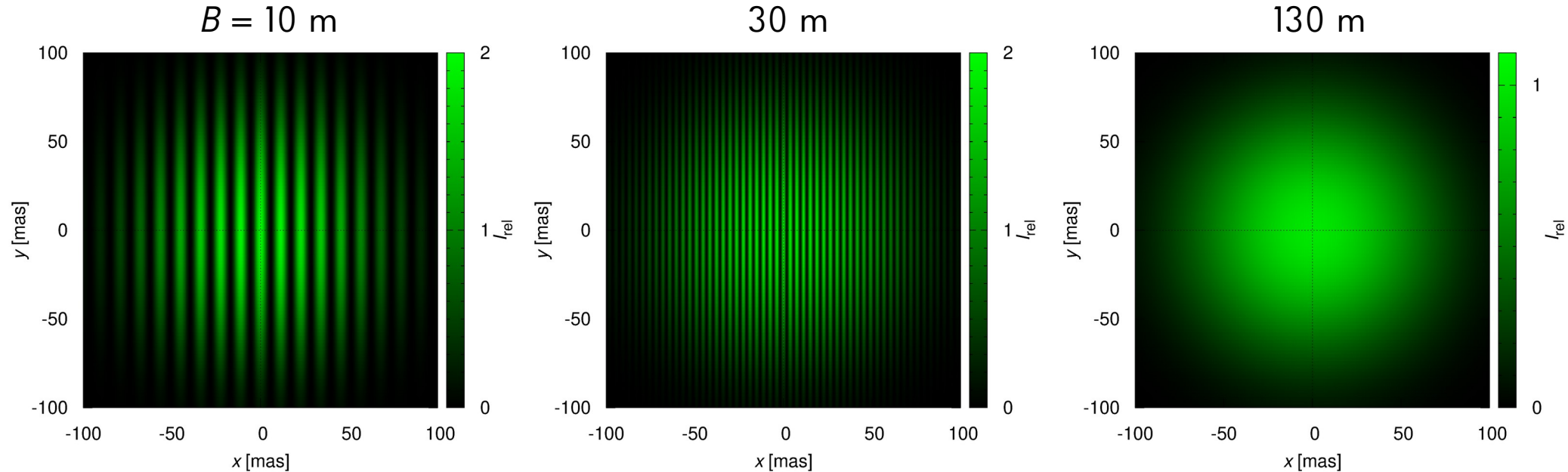
Dispersion

Vacuum



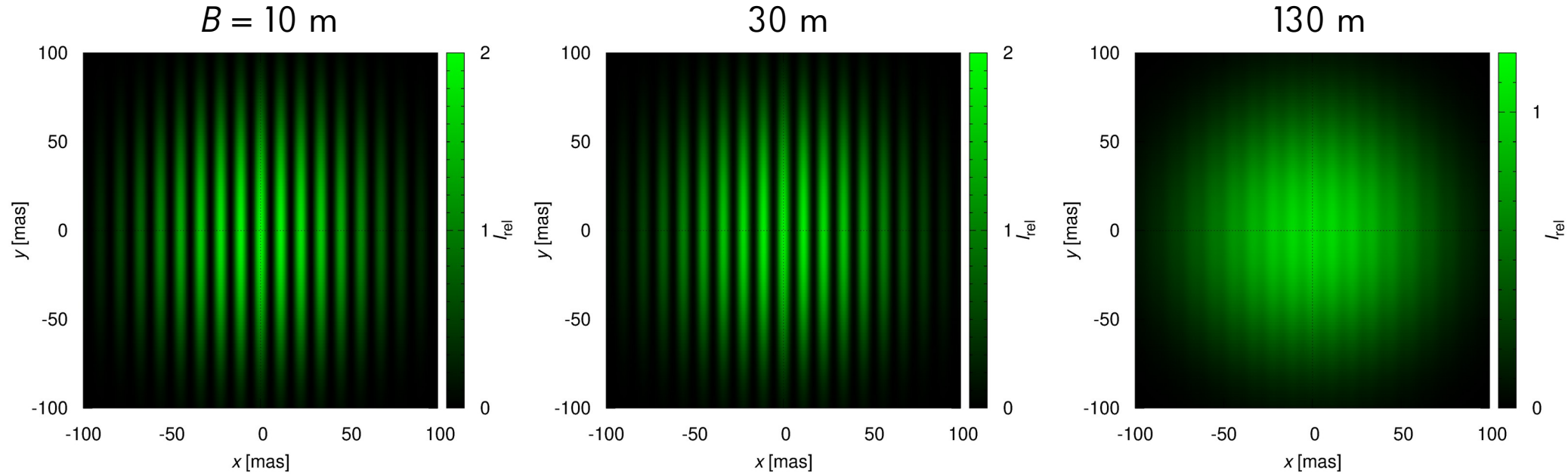
Fringes

- $D = 1 \text{ m}$, $B = 100 \text{ m}$, $\lambda = 550 \text{ nm}$, o. of a disc, $\theta = 1 \text{ mas}$, no seeing, no $\Delta\lambda_{\text{eff}}$, ...
- a drop in *visibility* (contrast) of fringes, i.e., the goal!

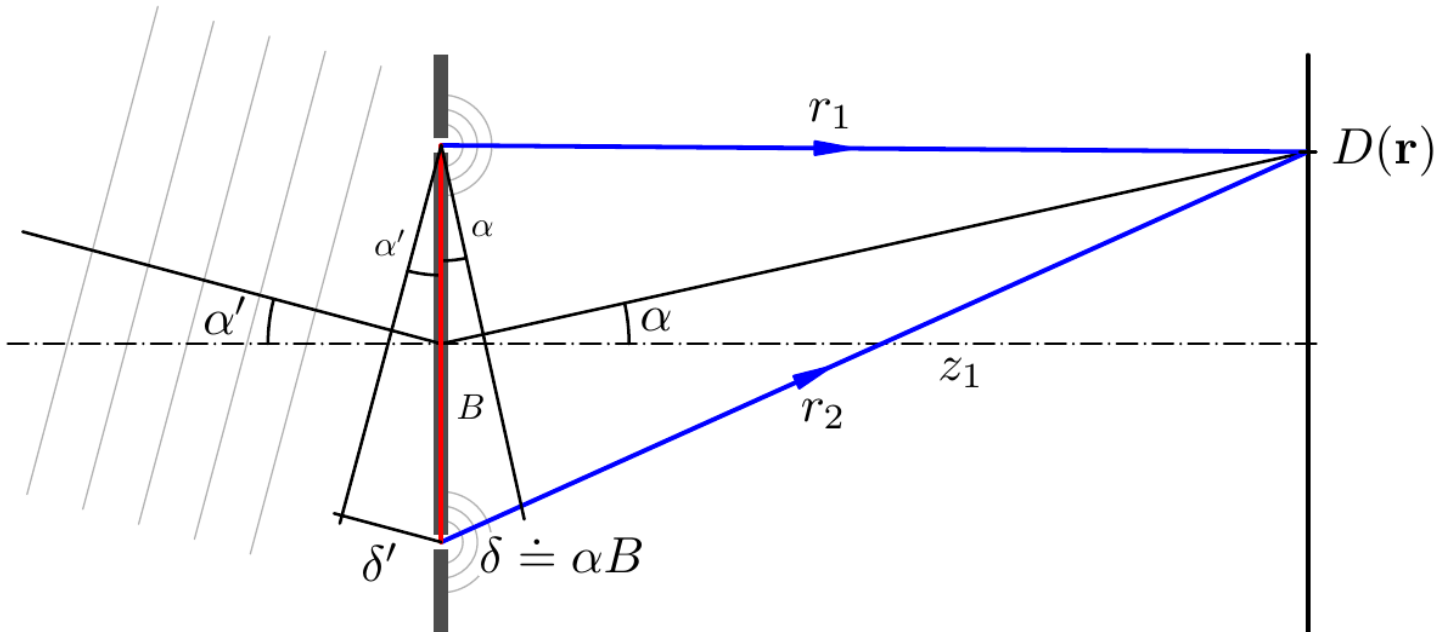


Fringes (cont.)

- delay line, periscopes → rearrangement of pupils (B vs. b) → constant # of f.



Fringes (cont.)



Obrázek 6.51: Uspořádání Youngova experimentu, kde B označuje vzájemnou vzdálenost štěrbin (základnu), z_1 vzdálenost stínítka od překážky, r_1 , r_2 vzdálenost studovaného místa na stínítku od štěrbin, α odpovídající odchylka od osy překážky, α' úhel dopadu vlny na překážku, δ , δ' dráhové rozdíly vznikající za a před překážkou.

van Cittert-Zernike theorem

- intensity I [1], angles α, α' [rad], wave number $k = 2\pi/\lambda$ [m^{-1}], baseline B [m]

$$I(\alpha, \alpha') = I_0 \{1 + \cos[k(\alpha + \alpha')B]\}, \quad (6.156)$$

$$I(\alpha) = \int I(\alpha, \alpha') d\alpha' = \overbrace{\int I(\alpha') d\alpha'}^{= I_0} + \overbrace{\int I(\alpha') \cos[k(\alpha + \alpha')B] d\alpha'}^{\Re[e^{ik\alpha B} \int I(\alpha') e^{ik\alpha' B} d\alpha']} , \quad (6.158)$$

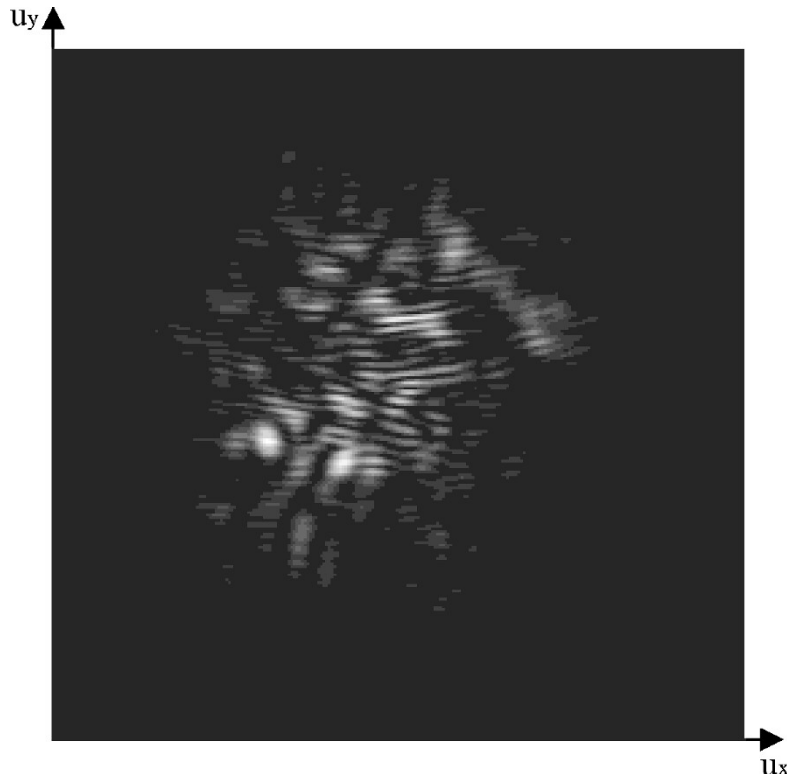
$$I(\vec{\alpha}) = I_0 \left\{ 1 + \Re \left[\mu(\vec{B}) e^{-ik\vec{\alpha} \cdot \vec{B}} \right] \right\} , \quad (6.159)$$

$$\mu(\vec{B}) \equiv \frac{\int I(\vec{\alpha}') e^{-ik\vec{\alpha}' \cdot \vec{B}} d\alpha'}{I_0} , \quad (6.160)$$

Interferometric observables

- complex visibility μ
- squared visibility $V^2 = \mu\mu^*$
- phase $\arg \mu$
- triple product $T_3 = \mu_{12} \mu_{23} \mu_{31}$
- closure phase $\arg T_3$
- triple product amplitude $|T_3|$
- differential visibility $\Delta V = \mu_{\lambda 1} \mu_{\lambda 2}$, approx. $V_{\lambda 1} \sim V_{\text{continuum}}$ (cf. Mourard et al. 2009)
- differential visibility amplitude $|\Delta V|$
- differential phase $\arg \Delta V$
- estimator $C_1 = 2E_{\text{fringe}}/E_{\text{speckle}}$, $E \equiv \int W df$ (Roddier & Lena 1984, Mourard et al. 1994)
- estimator $C_2 = 2W_{\text{fringe}}(f)/W_{\text{speckle}}(f - B/\lambda)$
- cross-spectrum $W_{12} = \langle F(I_{\lambda 1}) F(I_{\lambda 2})^* \rangle$ (Berio et al. 1999, 2001)
- ...

Interferometric observables



Berio et al. (1999)

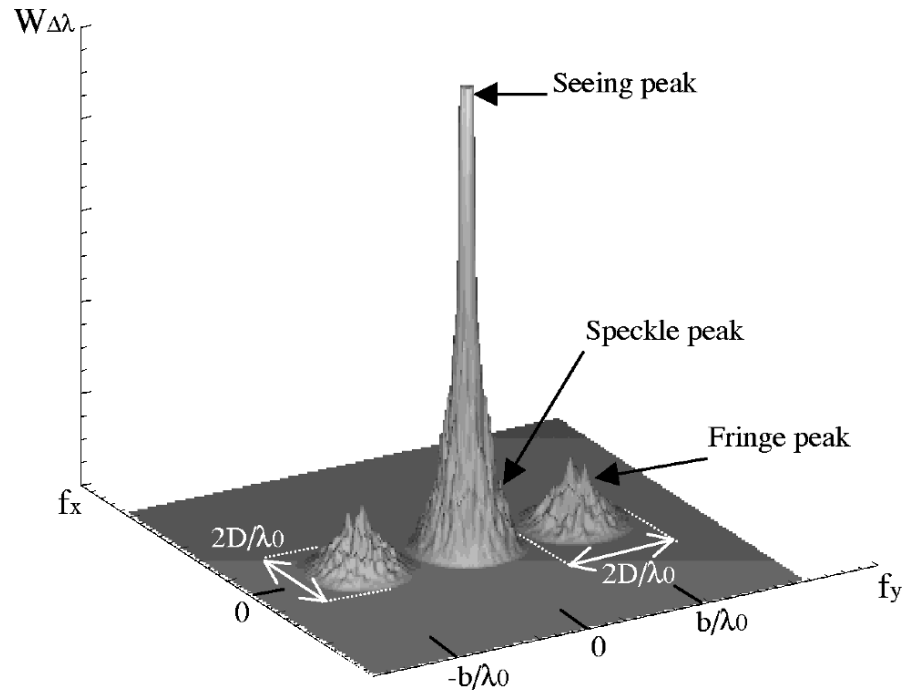


Fig. 1. Top, numerically simulated GI2T interferogram in the multichromatic mode and bottom, the corresponding spectral density. The fringe peaks are centered at $\pm b/\lambda_0$ because of the pupil rearrangement. (Coordinates are in arbitrary units.)

Model (Pyshellspec)

- + LTE level populations
- + LTE ionisation levels
- + 1D line-of-sight transfer
- + optically-thin (single) scattering ← no 3D, LI or ALI!
- non-isotropic scattering
- + prescribed ρ , T , v profiles
- + prescribed abundances
- + Voigt profile (prior to D.)
- + thermal broadening
- + microturbulence
- + natural
- + Stark
- + van der Waals
- + Doppler shift
- + HI bound-free continuum opacity
- + HI free-free
- + H⁻ bound-free,
- + H⁻ free-free
- Thomson scattering on free electrons
- Rayleigh scattering on neutral hydrogen
- Mie absorption on dust
- Mie scattering
- dust thermal emission
- line opacity
- + spherical primary (gainer)
- + Roche secondary (donor)
- black-body approximation (for *)
- + synthetic spectra (for *)
- irradiation
- reflection
- + limb darkening
- + gravity darkening
- heat transport

radiative
transfer

$$I_\nu(0) = \int_0^{\tau_\nu} S_\nu \, e^{-\tau'_\nu} \, d\tau'_\nu + I_\nu^\star(\nu_2) f_{\text{LD}} \, e^{-\tau_\nu}$$

limb darkening

$$S_\nu = \frac{\epsilon_\nu}{\chi_\nu}$$

$$\nu_2 = \nu \left(1 - \frac{v_z^\star}{c} \right)$$

$$\chi_\nu = \kappa_\nu + \sigma_\nu$$

$$\kappa_\nu = \kappa_\nu^{\text{line}} + \kappa_\nu^{\text{odf}} + \kappa_\nu^{\text{Hbf}} + \kappa_\nu^{\text{Hff}} + \kappa_\nu^{\text{H}^- \text{bf}} + \kappa_\nu^{\text{H}^- \text{ff}}$$

$$\sigma_\nu = \sigma_\nu^{\text{TS}} + \sigma_\nu^{\text{RS}}$$

scattering

$$\epsilon_\nu = \epsilon_\nu^{\text{th}} + \epsilon_\nu^{\text{sc}}$$

$$\epsilon_\nu^{\text{th}} = B_\nu(T(z)) \kappa_\nu$$

$$\epsilon_\nu^{\text{sc}} \doteq \sigma_\nu I_\nu^\star f_{\text{SH}} \frac{\omega}{4\pi}$$

shadowing

geometrical constraints

$$H(R) = h_{\text{cnb}} \sqrt{\frac{\gamma k_{\text{B}} T}{\mu m_{\text{u}}}} \frac{1}{\Omega_{\text{k}}}, \quad (11)$$

$$\Sigma(R) = \Sigma_{\text{nb}} \left(\frac{R}{R_{\text{innb}}} \right)^{e_{\text{densnb}}}, \quad (12)$$

$$\rho(R, 0) = \frac{\Sigma}{\sqrt{2\pi} H}, \quad (13)$$

$$\rho(R, z) = \rho(R, 0) \exp \left[-\min \left(\frac{z^2}{2H^2}; \frac{h_{\text{windnb}}^2}{2} \right) \right], \quad (14)$$

$$T(R, 0) = T_{\text{nb}} \left(\frac{R}{R_{\text{innb}}} \right)^{e_{\text{tmpnb}}}, \quad (15)$$

$$T(R, z) = T(R, 0) \max \left(1; 1 + (t_{\text{invnb}} - 1) \frac{|z| - h_{\text{invnb}} H}{a_{\text{neb}} H - h_{\text{invnb}} H} \right), \quad (16)$$

$$v_r(R) = \mathcal{H}(|z| - h_{\text{velnb}} H) v_{\text{nb}} \left(1 - \frac{R_{\text{innb}}}{R} \right)^{e_{\text{velnb}}}, \quad (17)$$

$$v_{\phi}(R) = \sqrt{\frac{GM_{\star}}{R}}, \quad (18)$$

$$\rho(R) = \rho_{\text{jt}} \left(\frac{R_{\text{injt}}}{R} \right)^2 \frac{v_r(R_{\text{injt}})}{v_r(R)} (1 \pm a_{\text{symjt}}), \quad (19)$$

$$T(R) = T_{\text{jt}} \left(\frac{R}{R_{\text{injt}}} \right)^{e_{\text{tmpjt}}}, \quad (20)$$

$$v_r(R) = v_{\text{jt}} \left(1 - \frac{R_{\text{cjt}}}{R} \right)^{e_{\text{veljt}}}, \quad (21)$$

$$\rho(R) = \rho_{\text{sh}} \left(\frac{R_{\text{insh}}}{R} \right)^2 \frac{v_r(R_{\text{insh}})}{v_r(R)}, \quad (22)$$

$$T(R) = T_{\text{sh}} \left(\frac{R}{R_{\text{insh}}} \right)^{e_{\text{tmpsh}}}, \quad (23)$$

$$v_r(R) = v_{\text{sh}} \left(1 - \frac{R_{\text{csh}}}{R} \right)^{e_{\text{velsh}}}. \quad (24)$$

$$\chi^2 = \chi_{\text{lc}}^2 + \chi_{\text{vis}}^2 + \chi_{\text{clo}}^2 + \chi_{\text{t3}}^2 + \chi_{\text{sed}}^2 + \chi_{\text{spe}}^2 + \chi_{\text{vamp}}^2 + \chi_{\text{vphi}}^2, \quad (1)$$

χ^2 terms

$$\chi_{\text{lc}}^2 = \sum_{k=1}^{N_{\text{band}}} \sum_{i=1}^{N_{\text{lc},k}} \left(\frac{m_{ki}^{\text{obs}} - m_{ki}^{\text{syn}}}{\sigma_{ki}} \right)^2, \quad (2)$$

$$\chi_{\text{vis}}^2 = \sum_{i=1}^{N_{\text{vis}}} \left(\frac{|V_i^{\text{obs}}|^2 - |V_i^{\text{syn}}|^2}{\sigma_i} \right)^2, \quad (3)$$

$$\chi_{\text{clo}}^2 = \sum_{i=1}^{N_{\text{clo}}} \left(\frac{\arg T_{3i}^{\text{obs}} - \arg T_{3i}^{\text{syn}}}{\sigma_i} \right)^2, \quad (4)$$

$$\chi_{\text{t3}}^2 = \sum_{i=1}^{N_{\text{clo}}} \left(\frac{|T_{3i}|^{\text{obs}} - |T_{3i}|^{\text{syn}}}{\sigma_i} \right)^2, \quad (5)$$

$$\chi_{\text{sed}}^2 = \sum_{i=1}^{N_{\text{sed}}} \left(\frac{F_{\lambda i}^{\text{obs}} - F_{\lambda i}^{\text{syn}}}{\sigma_i} \right)^2, \quad (6)$$

$$\chi_{\text{spe}}^2 = \sum_{i=1}^{N_{\text{spe}}} \left(\frac{I_{\lambda i}^{\text{obs}} - I_{\lambda i}^{\text{syn}}}{\sigma_i} \right)^2, \quad (7)$$

$$\chi_{\text{vamp}}^2 = \sum_{k=1}^{N_{\text{set}}} \sum_{i=1}^{N_{\text{vamp},k}} \left(\frac{V_i^{\text{obs}} - V_i^{\text{syn}} f_k}{\sigma_i} \right)^2, \quad (8)$$

$$\chi_{\text{vphi}}^2 = \sum_{k=1}^{N_{\text{set}}} \sum_{i=1}^{N_{\text{vphi},k}} \left(\frac{\arg V_i^{\text{obs}} - \arg V_i^{\text{syn}} + g_k + h_k}{\sigma_i} \right)^2, \quad (9)$$

Model (cont.)

- <http://sirrah.troja.mff.cuni.cz/~mira/betalyr/>
- Shellspec + Python = Pyshellspec (J. Budaj, J. Nemravová)
- calculation of interferometric observables (DFT), of χ^2
- multiprocessing module (split along λ ; 4-16 cores)
- discretisation $N_x = 160$, $N_y = 60$ ($\sim 1 R_\odot$); variable in z ($\sim \tau$)
- local & global optimisation (simplex, differential evolution, ...)
- 1 iteration: 2392 synthetic images (3 min)
- 1 convergence: $> 10^3$ steps (1 week)
- free parameters: i , Ω , d , T_{cp} , T_{nb} , T_{invnb} , ϱ_{nb} , R_{innb} , R_{outnb} , h_{invnb} , h_{windnb} , h_{cnb} , h_{shdnb} , v_{nb} , v_{trbnb} , e_{dennb} , e_{tmpnb} , e_{velnb} , etc. other objects, ...
- fixed parameters: P , $a \sin i$, e , ω , γ , JD_{min} , M_1 , $q = M_1/M_2$, f_{ill} , R_{star} , T_{star} , d_{gcp} , h_{velnb} , ...

```
#!/usr/bin/env python

import pyshellspec
...
# constants
ra = (18. + 50. / 60. + 4.79525 / 3600.) * 360./24.
dec = 33. + 21. / 60. + 45.6100 / 3600.
dir_data = '/home/mira/a/betalyr_MYTETEST/data_20171126'

def main():

    # data from MIRC
    obs = []
    dir = os.path.join(dir_data, 'mirc2017')
    infile = os.path.join(dir, 'mirc.ascii.lis')
    names = read_if(infile)
    for i in range(0, len(names)):
        print names[i]
        obs.append(pyshellspec.IFData(filename=os.path.join(dir, names[i]),
                                       location='chara', ra=ra, dec=dec,
                                       format='ascii', weight_vis2=0.5, weight_t3amp=0.5))
    ...

    # construct data class
    data = pyshellspec.Data(obs)

    # construct the model
    central = pyshellspec.CentralObject()
    companion = pyshellspec.Companion()
    disk = pyshellspec.Disk()
    nebula = pyshellspec.Nebula()
    orbit = pyshellspec.Orbit()
    objs = [central, companion, disk, nebula, orbit]
    model = pyshellspec.Model(objects=objs)

    # construct the Interface
    itf = pyshellspec.Interface(model=model, data=data, ncpu=4, image_size=180,
                                if_phase_precision=3, lc_phase_precision=2,
                                if_ew_precision=7, lc_ew_precision=9,
                                shellspec_template="template.in", use_offset=True)

    # set grid resolution
    itf.set_parameter('steps', value=1.0)
    itf.set_parameter('stepf', value=1.0)
    itf.set_parameter('stepsz', value=1.0)
    itf.set_parameter('stepfz', value=1.0)
```

```

# set shellspec parameters
itf.set_parameter('inebl', value=1) # nebula
itf.set_parameter('itnb', value=3) # power-law
itf.set_parameter('ichemc', value=1)
itf.set_parameter('ielnd', value=1)
itf.set_parameter('ithom', value=1) # scattering
itf.set_parameter('irayl', value=1)
itf.set_parameter('imie', value=0)
itf.set_parameter('imiepf', value=0)
itf.set_parameter('ishdnb', value=1) # shadowing
itf.set_parameter('iinvnb', value=2) # inversion of T
itf.set_parameter('iline', value=1)

# set fitted parameters
itf.set_parameter('routnb' , value=32.01701171 , fitted=True, vmin=26., vmax=35.)
itf.set_parameter('hinvnb' , value=7.213479944 , fitted=True, vmin=1.0, vmax=9.0)
itf.set_parameter('tinvnb' , value=1.965635409 , fitted=True, vmin=1.0, vmax=9.0)
itf.set_parameter('hwindnb' , value=4.300571244 , fitted=True, vmin=3.0, vmax=9.0)
itf.set_parameter('hcnb' , value=2.641315033 , fitted=True, vmin=1.0, vmax=15.0)
itf.set_parameter('hshdnb' , value=3.398141341 , fitted=False, vmin=1.0, vmax=12.0)
itf.set_parameter('tempnb' , value=33755.73450 , fitted=True, vmin=23000., vmax=34000.)
itf.set_parameter('densnb' , value=4.91712e-06 , fitted=True, vmin=2e-8, vmax=5e-6)
itf.set_parameter('edennb' , value=-3.092256032 , fitted=True, vmin=-3.5, vmax=-0.8)
itf.set_parameter('etmpnb' , value=-1.005127838 , fitted=True, vmin=-1.1, vmax=-0.70)
itf.set_parameter('dinc' , value=93.64153194 , fitted=True, vmin=91., vmax=97.)
itf.set_parameter('omega_an' , value=254.3871116 , fitted=True, vmin=252., vmax=255.)
itf.set_parameter('dd' , value=321.7816453 , fitted=True, vmin=305., vmax=330.)
itf.set_parameter('aneb' , value=9.0 , fitted=False, vmin=3.0, vmax=12.0)
itf.set_parameter('asini' , value=58.19 , fitted=False, vmin=53., vmax=63.)
itf.set_parameter('tempcp' , value=13300 , fitted=False, vmin=12000., vmax=14600.)

# compute one/fit
itf.compute_chi2(verbose=True)
# itf.run_fit(fitter='nlopt_nelder_mead', ftol=1e-6, maxiter=10000)
# itf.run_fit(fitter='sp_diff_evol', tol=1e-2, maxiter=10000)

itf.set_model_to_shellspec()
itf.write_template( final.in')
itf.write_iterations()
itf.write_model()

print "Note: fit.py ended successfully."
sys.exit(0)

if __name__ == '__main__':
    main()

```

convergence
by simplex

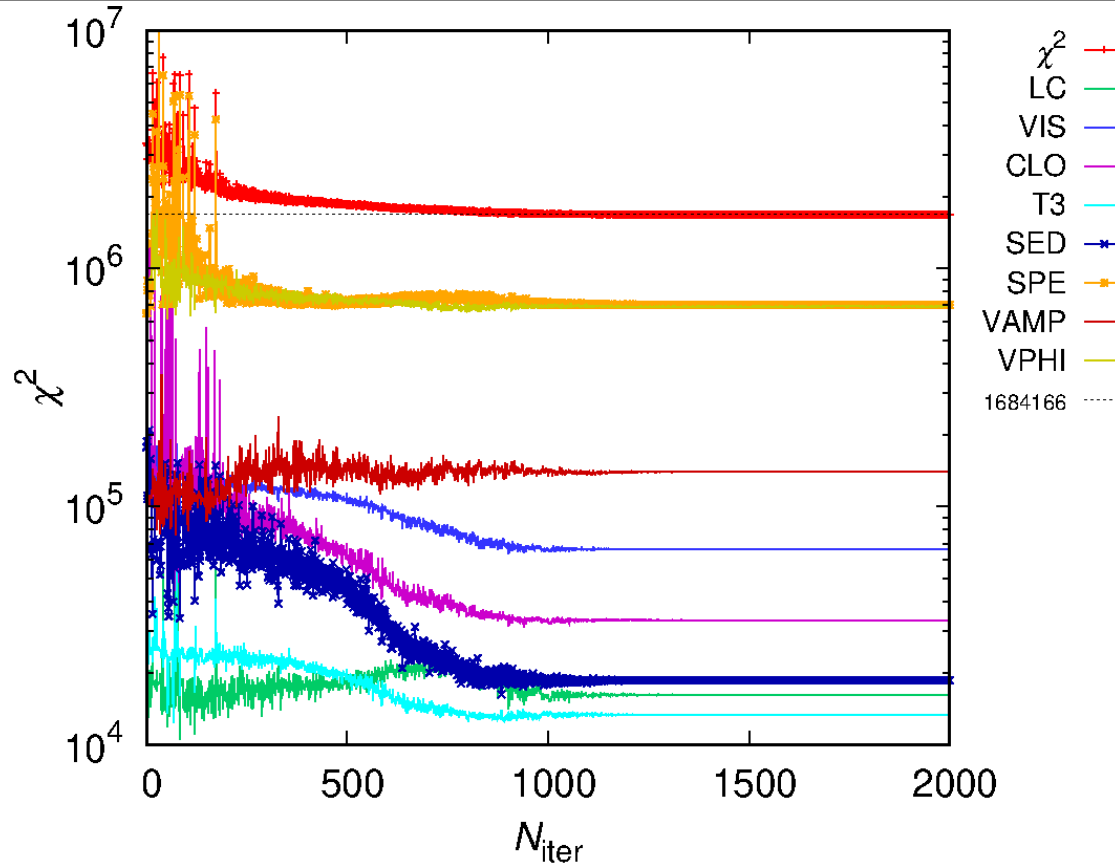
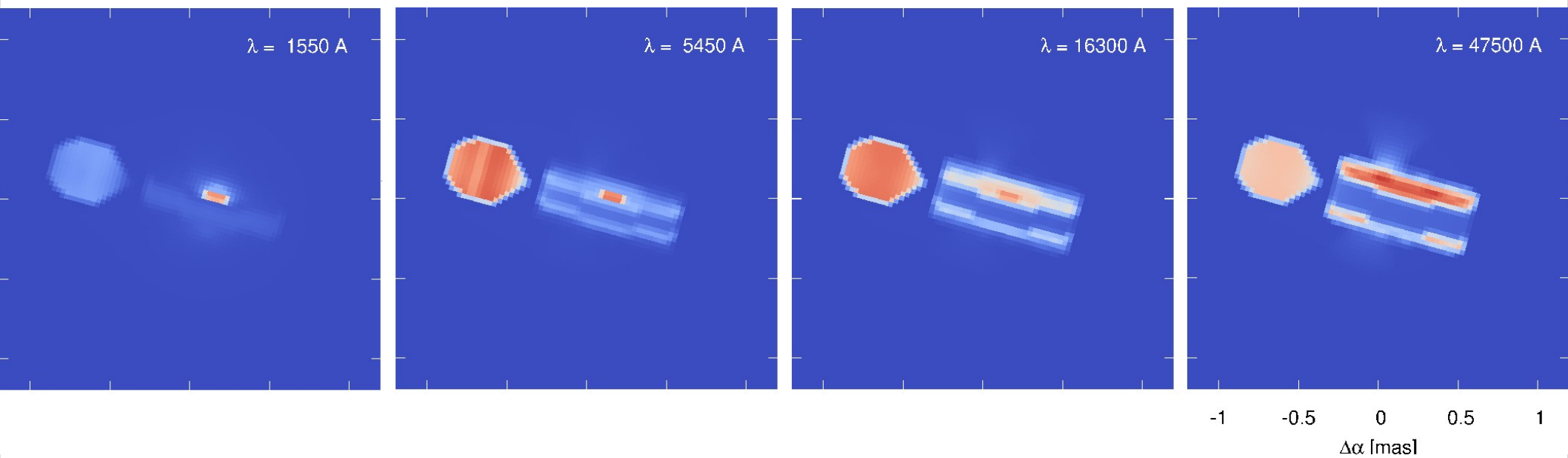


Fig. 6. χ^2 convergence (red) for joint model; individual contributions (LC, VIS, CLO, T3, SED, SPE, VAMP, VPHI) are also indicated. The model successfully converges to a local minimum. Some datasets have a substantially larger number of observations, (i.e. effectively a larger weight). The χ^2 values are different from Table 1 because the model was re-converged several times, and uncertainties of some datasets were modified.

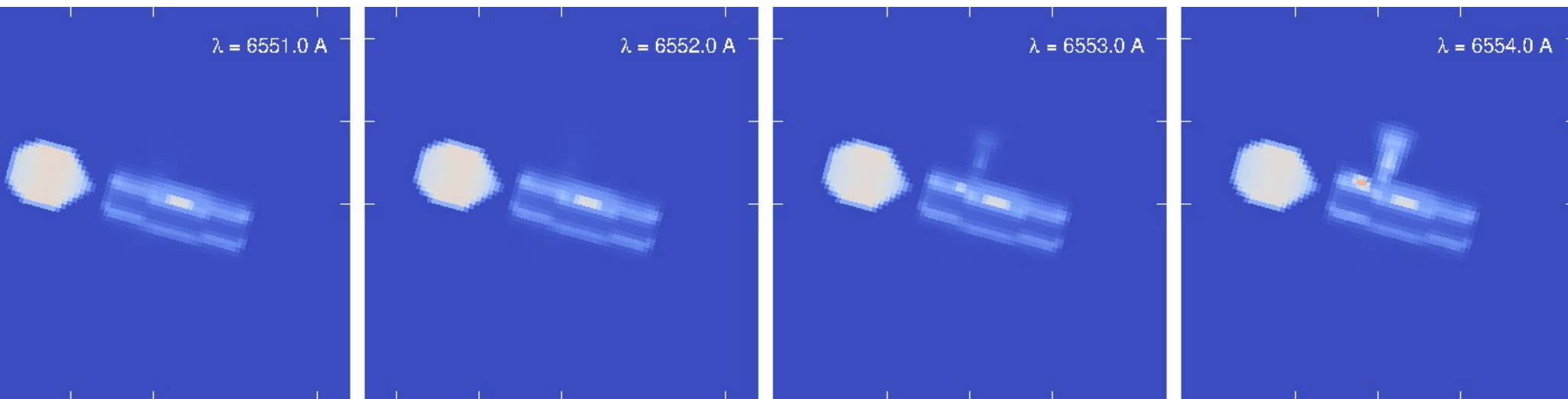
Continuum images

- NUV → FIR, optically thick



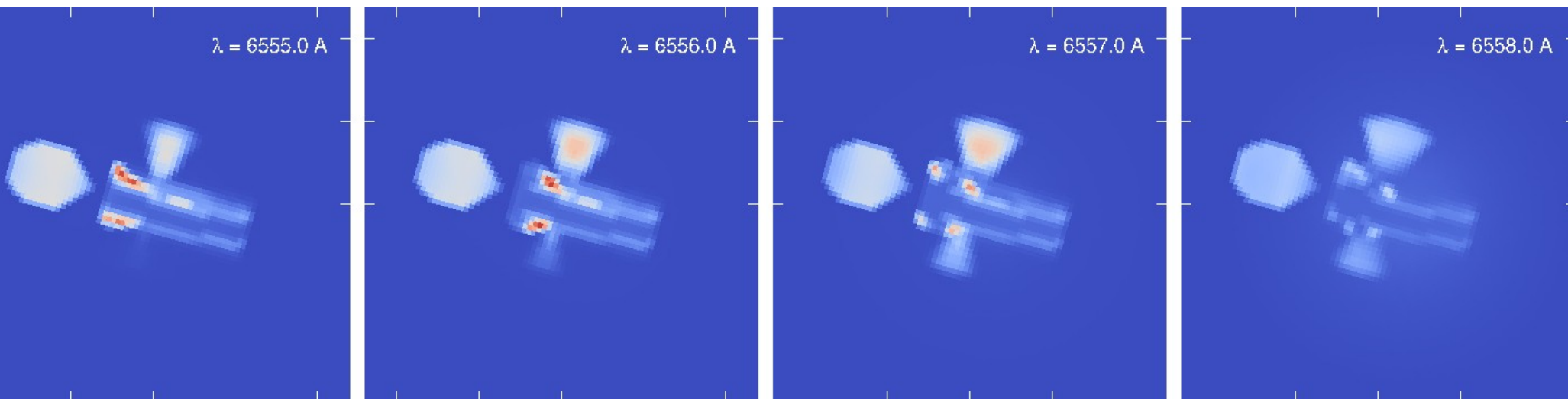
Line images

- H α , optically thin



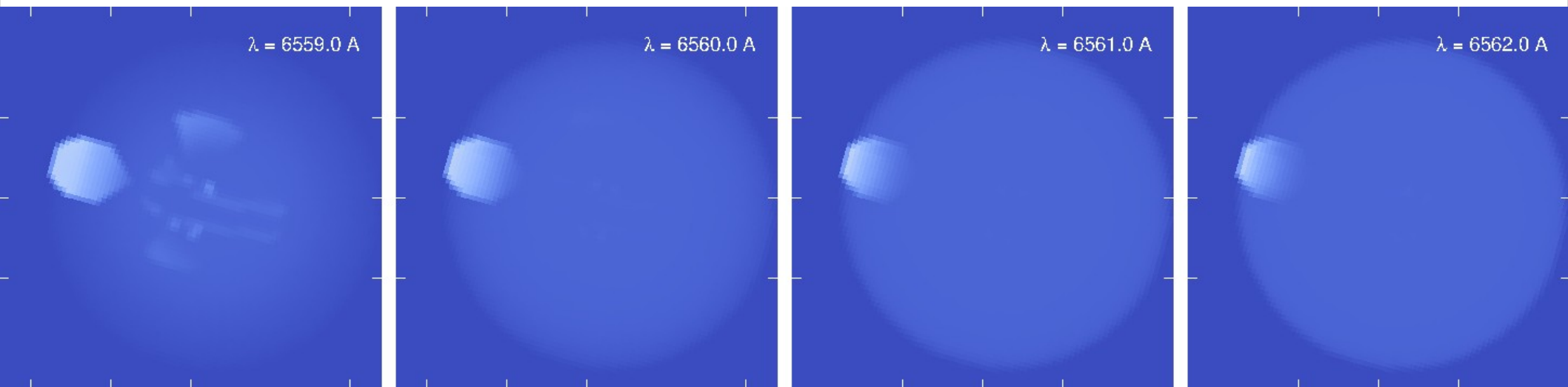
Line images

- H α , optically thin



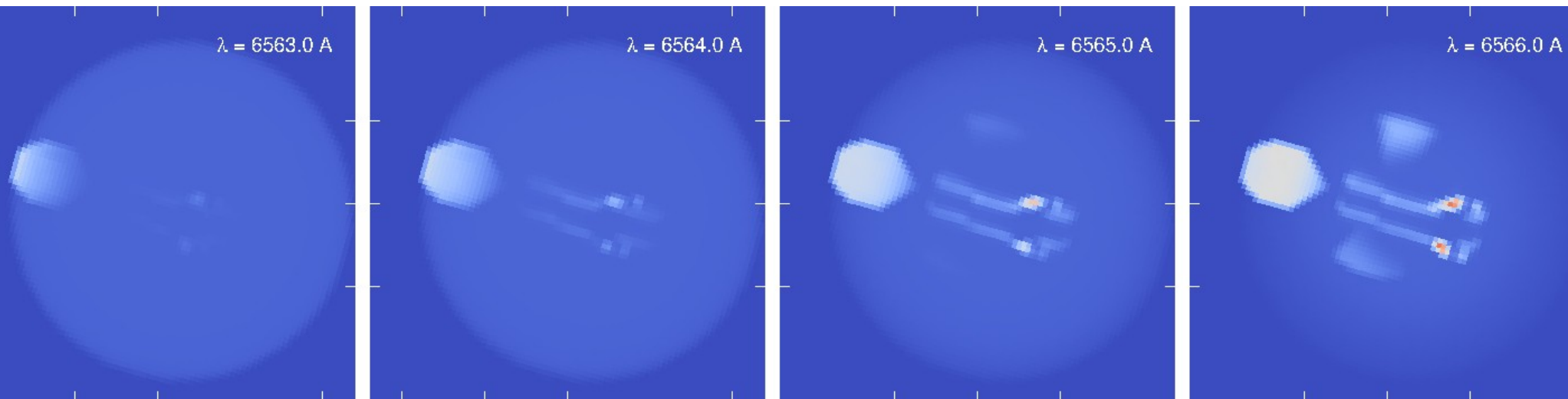
Line images

- H α , optically thin



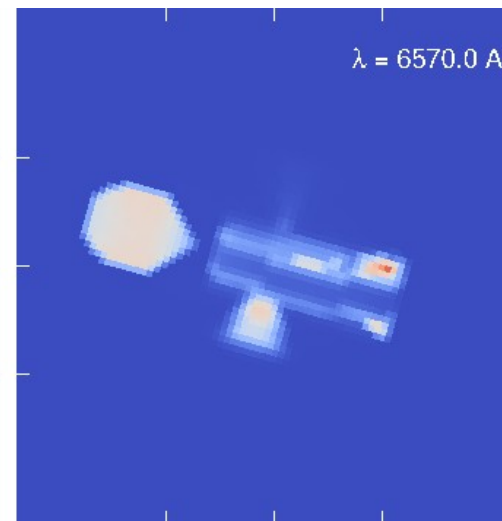
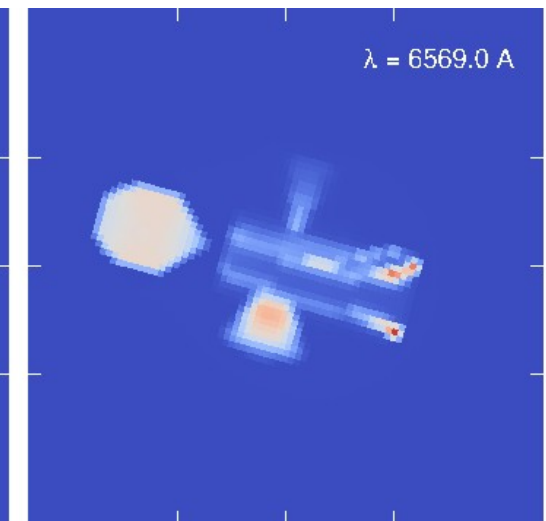
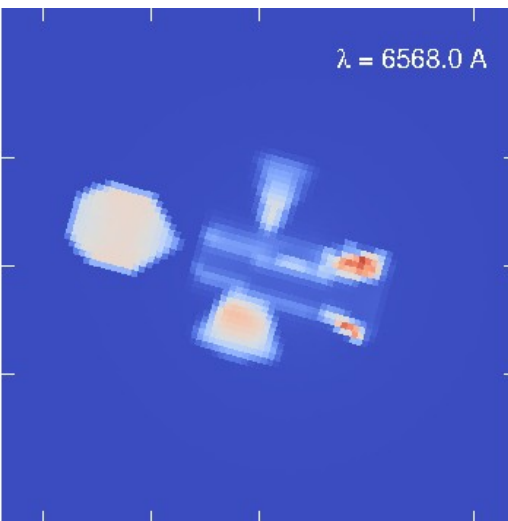
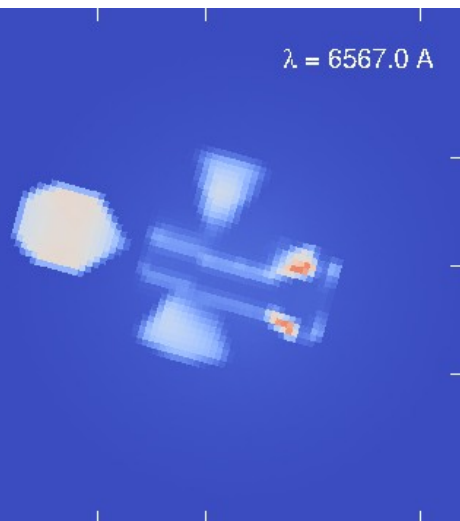
Line images

- H α , optically thin



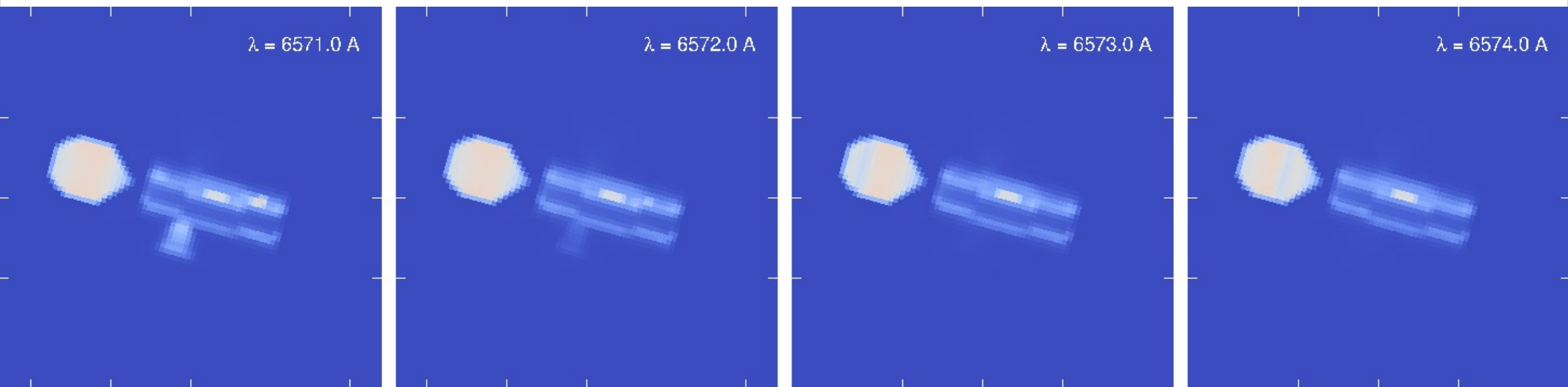
Line images

- H α , optically thin



Line images

- H α , optically thin



Observation-specific model(s)

- a ‘tension’ between datasets, cf. unconstrained parameters, cf. limits of p.

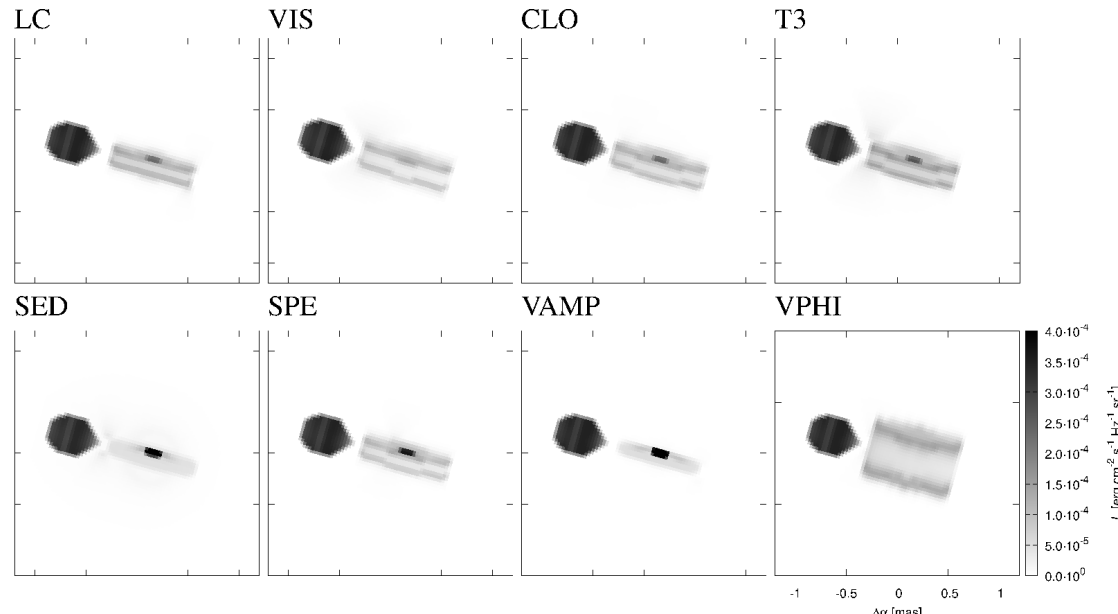


Fig. 18. Continuum synthetic images for observation-specific models (datasets LC, VIS, CLO, T3, SED, SPE, VAMP, and VPHI) for the wavelength 545 nm (V). The apparent differences (e.g. the thickness of the disc, the appearance of the primary) demonstrate systematics between datasets. Alternately, some datasets (e.g. VPHI) do not constrain certain parameters.

Differential visibility

- if visibility decreases (across H α) → size must increase...

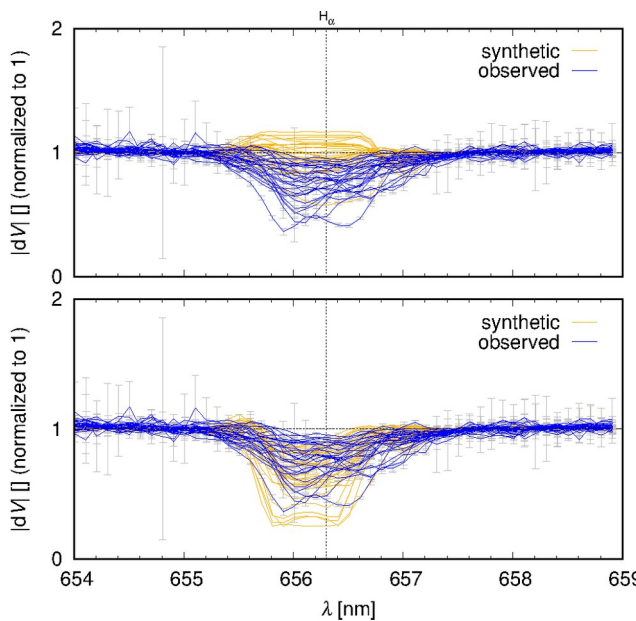


Fig. 5. Observed differential visibility amplitude $|dV|$ versus wavelength λ , normalised to 1 in the continuum (blue), and its decrease across the H α profile. Uncertainties of $|dV|$ are also plotted (grey). Synthetic visibilities (yellow) are shown for the two “extreme” values of the shell’s outer radius $R_{\text{outsh}} = 40 R_\odot$ (top) and $120 R_\odot$ (bottom).

Chemical composition

- if $H\alpha$ is in emission \rightarrow CII must be in emission...

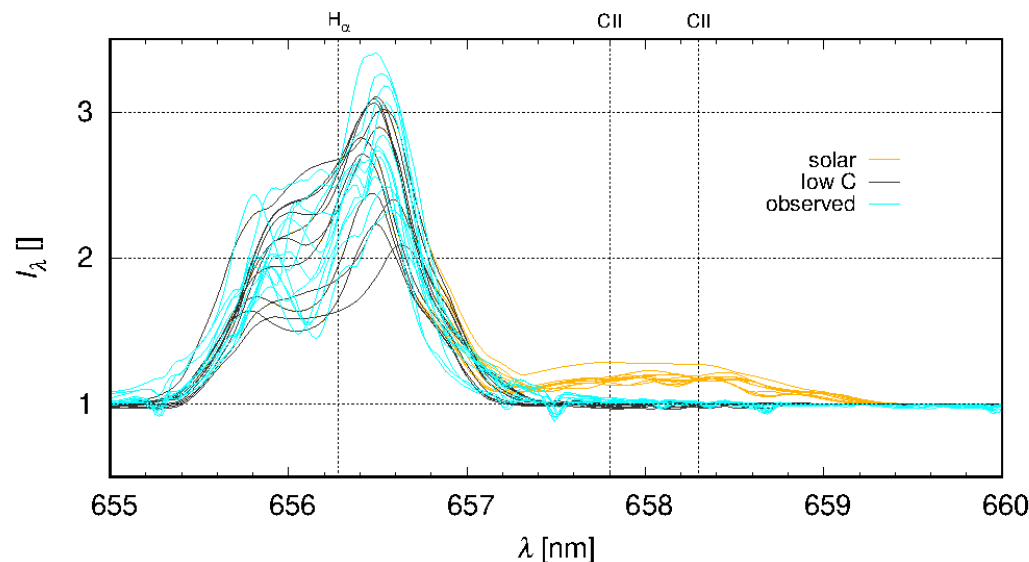
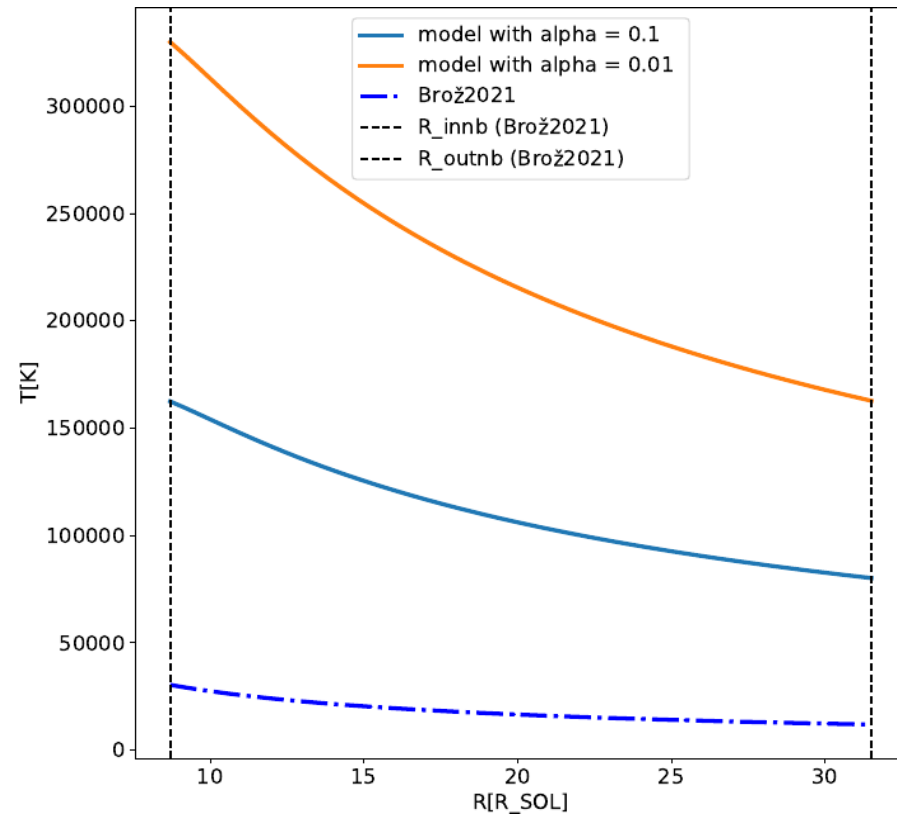
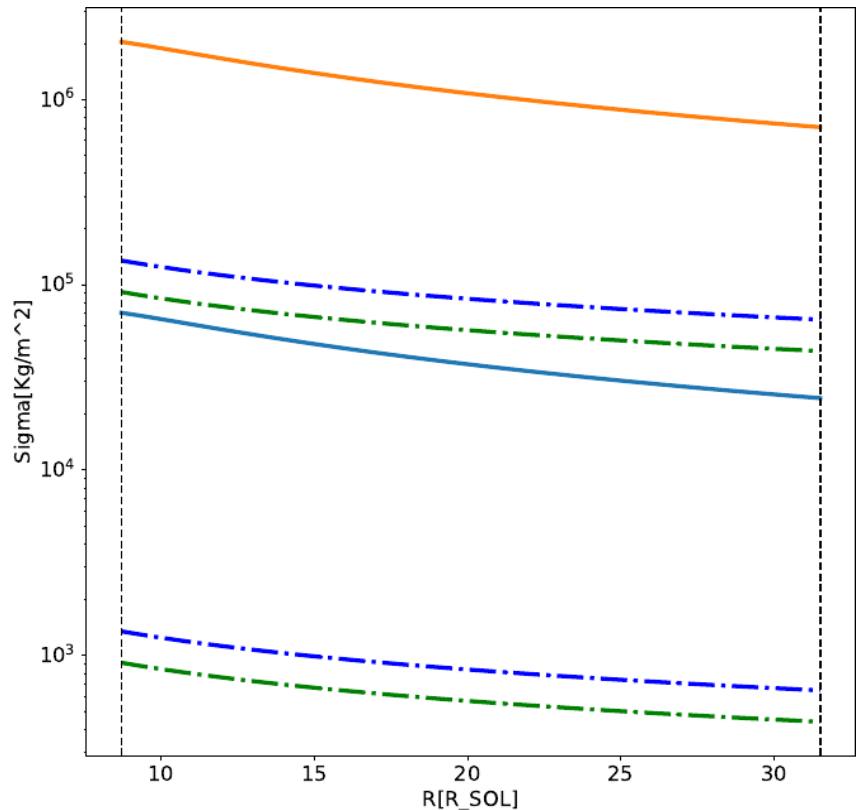


Fig. 20. Synthetic spectra for solar abundances (yellow) and 10^{-2} lower abundance of C (grey); observed spectra (blue) are plotted for comparison. For the solar composition, C II 6578 and 6583 emission is too strong.

Vitovský (in prep.)

- analytical accretion disk of Shakura & Sunyaev (1973), w. viscosity $\nu = \alpha c_s H$
- modified for a *general* opacity prescription $\kappa = \kappa_0 \rho^A T^B$
- constrained by the accretion rate of β Lyr A, $dM/dt = 2 \cdot 10^{-5} M_{\odot} \text{ yr}^{-1}$
- radial profiles $\Sigma(r)$, $T(r)$, $H(r)$ compared to “observations” (Brož et al. 2021)
- most models excluded due to self-consistency (P_{gas} vs. P_{rad}); κ is Kramers
- Σ must be much higher! 10000 kg m^{-2} at the inner rim, if $\alpha = 0.1$
- T must be much higher! 10^5 K in the mid-plane
- cf. vertical scale height H is hydrostatic (low μ)
- steep vertical gradient & inversion in disk atmosphere?



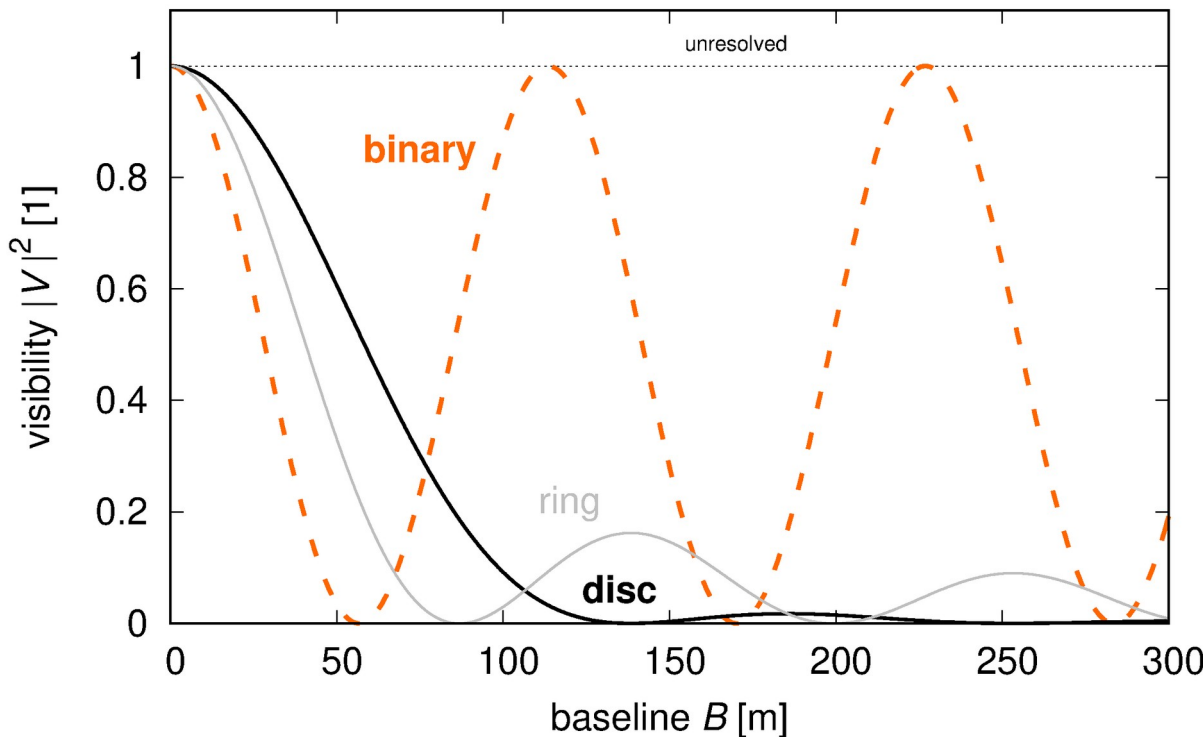
model with alpha = 0.1	model with alpha = 0.01
Brož2021	Brož2021 (Rho x 100)
Vertically hydrostatic model	Vertically hydrostatic model (Rho x 100)
---	---
R_innb (Brož 2021)	R_outnb (Brož 2021)

Caveats

- Is (u, v) coverage sufficient? 1 visibility \sim 1 pixel
- Is a^* resolved? (cf. Airy)
- Is a^* in the aperture?
- What is the *state* of instrument?
- Is a model sufficient?
- Is a model resolution-dependent?
- Adding an optically-thin object changes other objects!
- Some parameters seem to be more important than expected (e.g., v_{turb}).
- A ‘tension’ between individual datasets (LC, VIS, CLO, T3, SED, SPE, VAMP, VPHI)?
- Not-so-successful models are often useful to exclude...

Simple i. models

- binaries, multiple *, uniform disk(s), limb-darkened d., ring, ... cf. combinations!



Model (χ_{tau})

- + multiple * systems
 - + N-body perturbations
 - + resonances, ...
 - + stability!
 - + oblateness
 - + multipoles ($l = 10$)
 - + parametrized post-Newtonian (PPN)
 - + internal tides
 - + external tides
 - “brute-force”
 - variable geometry
 - + fitting of orbits
 - + fitting of radiative parameters
 - fitting of shapes
 - + simplex
 - + subplex
 - annealing
- 1. astrometry (SKY)
 - 2. differential astrometry (SKY2)
 - 3. angular velocity (SKY3)
 - 4. radial velocity (RV)
 - 5. transit-timing variations (TTV)
 - 6. eclipse duration (ECL)
 - 7. visibility (VIS)
 - 8. closure-phase (CLO)
 - 9. triple product (T3)
 - 10. light curve, u. Wilson-Devinney (LC)
 - 11. light curve, u. polygonal (LC2)
 - 12. synthetic spectra (SYN)
 - 13. spectral-energy distribution (SED)
 - 14. adaptive-optics silhouettes (AO)
 - 15. adaptive-optics imaging (AO2)
 - 16. occultations (OCC)

N-body
terms

$$f = - \sum_{j \neq i}^N \frac{Gm_j}{r_{ij}^3} \mathbf{r}_{ij} + f_{\text{ppn}} + f_{\text{oblat}} + f_{\text{multipole}} + f_{\text{tides}}.$$

$$\begin{aligned} \mathbf{f}_{\text{ppn}} = & \sum_{j \neq i}^N [-K_1(K_2 + K_3 + K_4 + K_5 + K_6 + K_7 + K_8) \mathbf{r}_{ij} \\ & + K_1(K_9 + K_{10}) \dot{\mathbf{r}}_{ij} + K_{11} \ddot{\mathbf{r}}_j], \end{aligned} \quad (2)$$

$$K_1 = \frac{1}{c^2} \frac{Gm_j}{r_{ij}^3}, \quad (3)$$

$$K_2 = -2(\beta + \gamma) \sum_{k \neq i} \frac{Gm_k}{r_{ik}}, \quad (4)$$

$$K_3 = -(2\beta - 1) \sum_{k \neq j} \frac{Gm_k}{r_{jk}}, \quad (5)$$

$$K_4 = \gamma v_i^2, \quad (6)$$

$$K_5 = (1 + \gamma) v_j^2, \quad (7)$$

$$K_6 = -2(1 + \gamma) \dot{\mathbf{r}}_i \cdot \dot{\mathbf{r}}_j, \quad (8)$$

$$K_7 = -\frac{3}{2} \frac{(\mathbf{r}_{ij} \cdot \dot{\mathbf{r}}_j)^2}{r_{ij}^2}, \quad (9)$$

$$K_8 = \frac{1}{2} \mathbf{r}_{ji} \cdot \ddot{\mathbf{r}}_j, \quad (10)$$

$$K_9 = (2 + 2\gamma) \mathbf{r}_{ij} \cdot \dot{\mathbf{r}}_i, \quad (11)$$

$$K_{10} = -(1 + 2\gamma) \mathbf{r}_{ij} \cdot \dot{\mathbf{r}}_j, \quad (12)$$

$$K_{11} = \frac{3 + 4\gamma}{2c^2} \frac{Gm_j}{r_{ij}}. \quad (13)$$

oblateness
precession

$$\boldsymbol{f}_{\text{oblat}} = - \sum_{j \neq i}^{N_{\text{bod}}} \frac{1}{2} k_{\text{L}j} \omega_{\text{rot}j}^2 \frac{\boldsymbol{R}_i^5}{\boldsymbol{r}_{ij}^5} \boldsymbol{r}_{ji}.$$

multipoles

$$U = -\frac{GM}{r} \sum_{\ell=0}^{N_{\text{pole}}} \left(\frac{R}{r}\right)^\ell \sum_{m=0}^{\ell} P_{\ell m}(\cos \theta) [C_{\ell m} \cos(m\phi) + S_{\ell m} \sin(m\phi)], \quad (8)$$

$$\frac{dU}{dr} = -GM \sum_{\ell=0}^{N_{\text{pole}}} R^\ell (-\ell - 1) r^{-\ell-2} \sum_{m=0}^{\ell} P_{\ell m}(\cos \theta) [C_{\ell m} \cos(m\phi) + S_{\ell m} \sin(m\phi)], \quad (9)$$

$$\frac{dU}{d\theta} = -GM \sum_{\ell=0}^{N_{\text{pole}}} R^\ell r^{-\ell-1} \sum_{m=0}^{\ell} P'_{\ell m}(\cos \theta) \sin \theta [C_{\ell m} \cos(m\phi) + S_{\ell m} \sin(m\phi)], \quad (10)$$

$$\frac{dU}{d\phi} = -GM \sum_{\ell=0}^{N_{\text{pole}}} R^\ell r^{-\ell-1} \sum_{m=0}^{\ell} P_{\ell m}(\cos \theta) [-C_{\ell m} \sin(m\phi)m + S_{\ell m} \cos(m\phi)m], \quad (11)$$

$$f_{\text{mp}} = -\left(\frac{dU}{dr}, \frac{1}{r} \frac{dU}{d\theta}, \frac{1}{r \sin \theta} \frac{dU}{d\phi} \right), \quad (12)$$

$$C_{\ell 0} = \frac{1}{MR^\ell} \rho \int_V |\mathbf{r}|^\ell P_\ell(\cos \theta) dV, \quad (13)$$

$$C_{\ell m} = \frac{2}{MR^\ell} \frac{(\ell - m)!}{(\ell + m)!} \rho \int_V |\mathbf{r}|^\ell P_{\ell m}(\cos \theta) \cos(m\phi) dV, \quad (14)$$

$$S_{\ell m} = \frac{2}{MR^\ell} \frac{(\ell - m)!}{(\ell + m)!} \rho \int_V |\mathbf{r}|^\ell P_{\ell m}(\cos \theta) \sin(m\phi) dV, \quad (15)$$

$$P_0(x) = 1, \quad P_1(x) = x, \quad P_2(x) = \frac{1}{2}(3x^2 - 1), \dots \quad (16)$$

$$P_{11}(x) = (1 - x^2)^{\frac{1}{2}}, \quad P_{21}(x) = 3x(1 - x^2)^{\frac{1}{2}}, \dots \quad (17)$$

tides
dissipation

$$f_{\text{tides}} = K_1 [K_2 \mathbf{r}' - K_3 \mathbf{r} - K_4(\mathbf{r} \times \boldsymbol{\omega} + \mathbf{v}) + K_5(K_6 \mathbf{r} - K_7 \mathbf{r}')], \quad (5)$$

$$K_1 = \frac{3Gm^\star R^5 k_2 \Delta t}{(r' r)^5}, \quad (6)$$

$$K_2 = \frac{5}{r'^2} \left[\mathbf{r}' \cdot \mathbf{r} (\mathbf{r} \cdot \boldsymbol{\omega} \times \mathbf{r}' + \mathbf{r}' \cdot \mathbf{v}) - \frac{1}{2r^2} \mathbf{r} \cdot \mathbf{v} (5(\mathbf{r}' \cdot \mathbf{r})^2 - r'^2 r^2) \right], \quad (7)$$

$$K_3 = \mathbf{r} \cdot \boldsymbol{\omega} \times \mathbf{r}' + \mathbf{r}' \cdot \mathbf{v}, \quad (8)$$

$$K_4 = \mathbf{r}' \cdot \mathbf{r}, \quad (9)$$

$$K_5 = \frac{\mathbf{r} \cdot \mathbf{v}}{r^2}, \quad (10)$$

$$K_6 = 5\mathbf{r}' \cdot \mathbf{r}, \quad (11)$$

$$K_7 = r^2, \quad (12)$$

$$\boldsymbol{\Gamma} = \mathbf{r} \times m' f_{\text{tides}}. \quad (13)$$

Brož et al. (2022, A&A 666, A24)

- HD 93206: Aa1, Aa2, Ac1, Ac2, Ab, Ad, B, C, D
- QZ Car: (Aa1+Aa2) + (Ac1+Ac2)
- data: SKY2, RV, TTV, SYN, SED, VIS, CLO, T3
- ESO archive: 098.D-0706(B), 099.D-0777(B)
- VLTI/GRAVITY pipeline (Freudling et al. 2013)
- $(u, v) \equiv B/\lambda$ coverage, of wide orbit
- nominal vs. alternative models ($\sim 130\text{-}140 M_{\odot}$)
- anomalous extinction? ($R_V = 3.4$, not 3.1)
- $d = 2800$ vs. 2450 pc

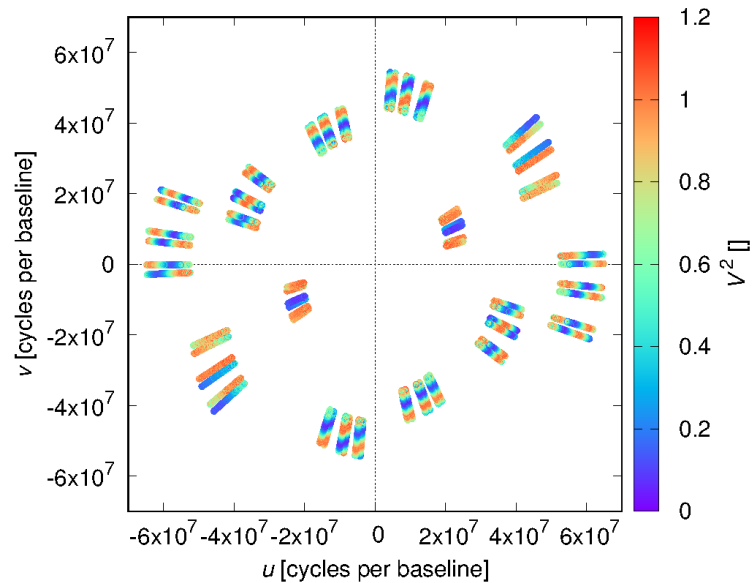


Fig. 3. Coverage $(u, v) \equiv B/\lambda$ (in cycles per baseline) of new interferometric observations (see Table 1). The corresponding squared visibility V^2 is plotted in colour (see colour bar at right). The wide orbit ((Ac1+Ac2)+(Aa1+Aa2)), having the angular separation more than 30 mas, is clearly resolved.

VLTI

- high S/N, many λ , either precise astrometry ($10 \mu\text{as}$), or fitting of V^2 , $\arg T_3$

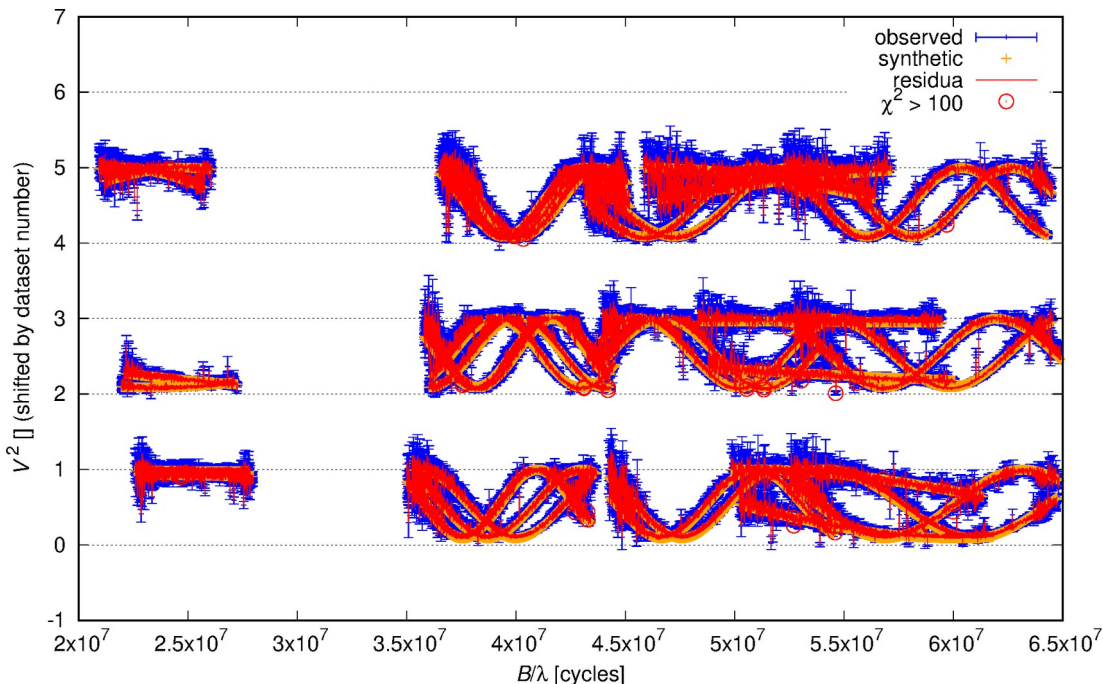


Fig. 12. Squared visibilities V^2 for VLTI/GRAVITY observations (March 14, 2017 and April 27, 2017; blue), synthetic V^2 (orange), and residuals (red). The sinusoidal dependence on the baseline B/λ essentially corresponds to a wide binary ((Ac1+Ac2)+(Aa1+Aa2)). Disks of individual stellar components cannot be resolved (at 0.08 mas, which correspond to a drop in V^2 of only 0.01 at the longest baseline).

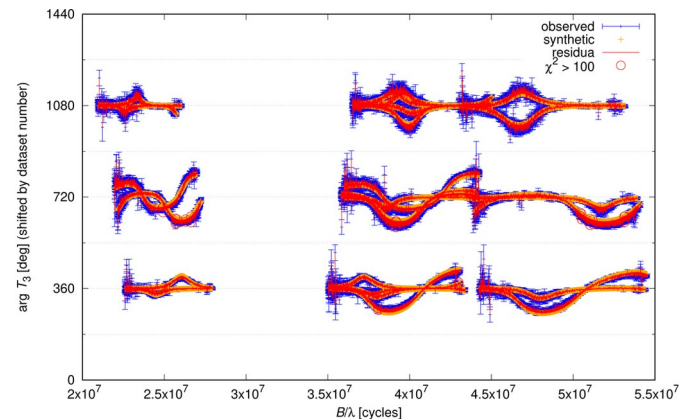


Fig. 13. Same as Fig. 12, but for the closure phase $\arg T_3$. Again, the dependence on B/λ is similar to that of a binary.

best-fit models
 convergence
 parameters m_1 vs. m_2
 contributions to χ^2
 correlations
 orthogonality

best fits
good fits
poor fits

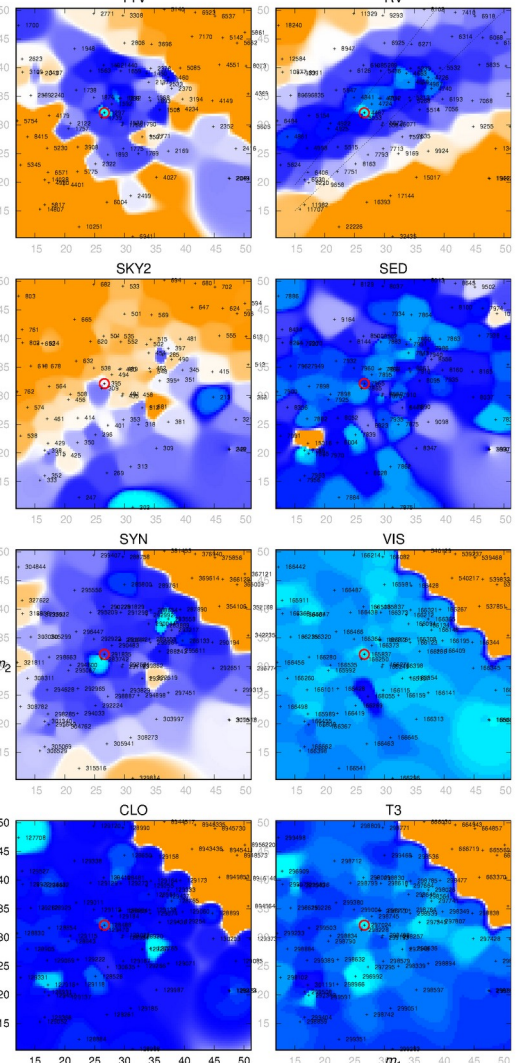


Fig. 5. Contributions to χ^2 for a set of 81 best-fit models. Individual contributions (datasets) are shown in the panels (from top left): TTV, RV, SKY2, SED, SYN, VIS, CLO, T3. Every convergence was initialized with a different combination of masses m_1 , m_2 (Ac1, Ac2) in the range $15\text{--}50 M_\odot$, while m_3 (Aa1) was set to $m_1 = m_2 = m_4$. All parameters were free during convergence. The axes correspond to the masses m_1 and m_2 ; the colours correspond to χ^2 (see also tiny numbers), with adapted colour scales: cyan best fits, blue good fits ($<1.2 \min \chi^2$), orange poor fits ($\geq 1.2 \min \chi^2$). The factor was 3.0 for TTV, RV, SKY2. The forbidden regions can be clearly seen (e.g., high m_1 , m_2 especially due to CLO), as well as correlations between the parameters (TTV \neg , RV \neg). The weighted best fit for all the datasets is denoted by the red circle.

Brož et al. (2023, A&A 676, A60)

- (22) Kalliope + Linus system
- data: SKY, AO, LC2
- cf. variable geometry
- speckle-interferometry: C2PU/PISCO, Calern, France
(Prieur et al. 1998, Scardia et al. 2019)
- $D = 1 \text{ m}$, $\lambda = 550 \text{ nm}$, 14 000 exposures, 100 ms;
processed by FT, averaging, i.e. FT (Labeyrie 1970)
- precision 7 mas, 6° (in PA)

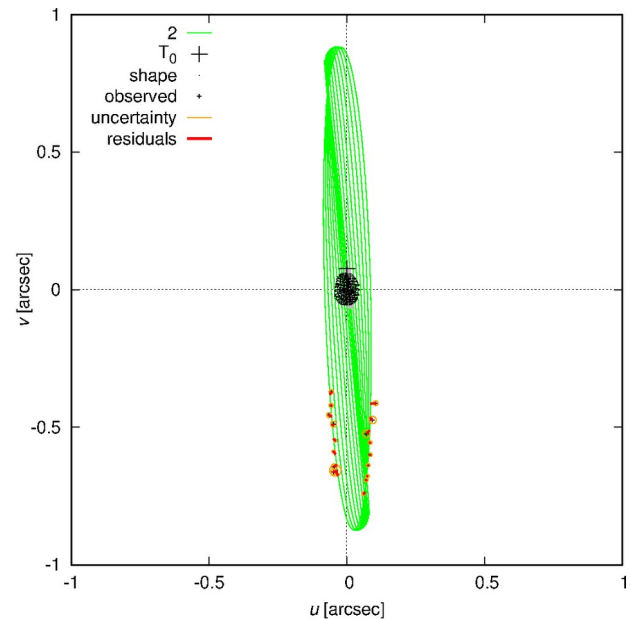


Fig. 9. Orbit of Linus in the (u, v) plane, derived from the short-arc astrometric + photometric model. It fits the PISCO dataset around 2459579, namely, close to the mutual occultation events, when the orbit is seen from the edge. The synthetic orbit of Linus (i.e., body 2) is plotted in green, the observed astrometry in yellow, the residuals in red, the shape of (22) in black. The viewing geometry is changing in the course of time; otherwise the orbit is elliptical. The position at the reference epoch T_0 is marked by the cross. The contribution to χ^2 is $\chi_{\text{sky}}^2 = 27$ and $n_{\text{sky}} = 36$.

Polygonal algorithm

1st clipping:
partial shadowing
2nd clipping:
partial visibility
'killed' d. errors

Vatti (1992)
Prša et al. (2016)
Clipper2 C++ library
structures¹
optimisations²

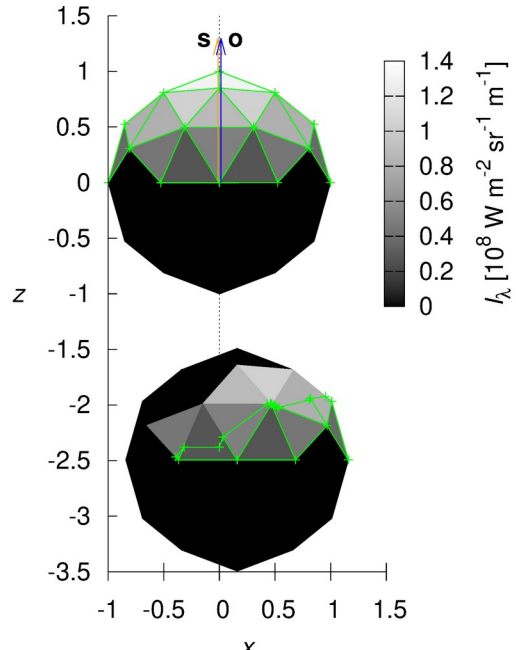


Fig. 1. Two-sphere test of the polygon light curve algorithm. We can even use a very coarse discretisation of 42 nodes for each sphere, because we compute partial eclipses, partial occultations, or partial transits. Shades of gray show the monochromatic intensity I_λ (in $\text{W m}^{-2} \text{ sr}^{-1} \text{ m}^{-1}$), green lines show the non-eclipsed and non-occulted polygons used to compute the surface areas. The orange arrow shows the direction towards the Sun and blue towards the observer. The test bodies are metre-sized, 1 au from the Sun and 1 au from the observer. See also Fig. 2.

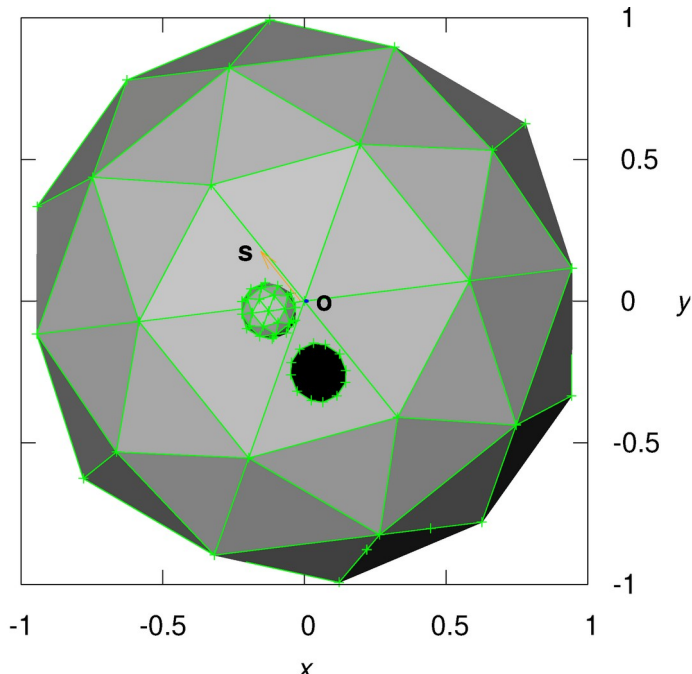


Fig. 3. Similar to Fig. 1. A tiny-triangle test, where one body is large and other body is small. It demonstrates that annular eclipses, as well as partial eclipses, partial occultations, and partial transits, are computed exactly. The polygon corresponding to the shadow (black) has a negative signed area.

¹ set of sets of polygons

² bounding-box tests

exact light curve
scattered light
Hapke law

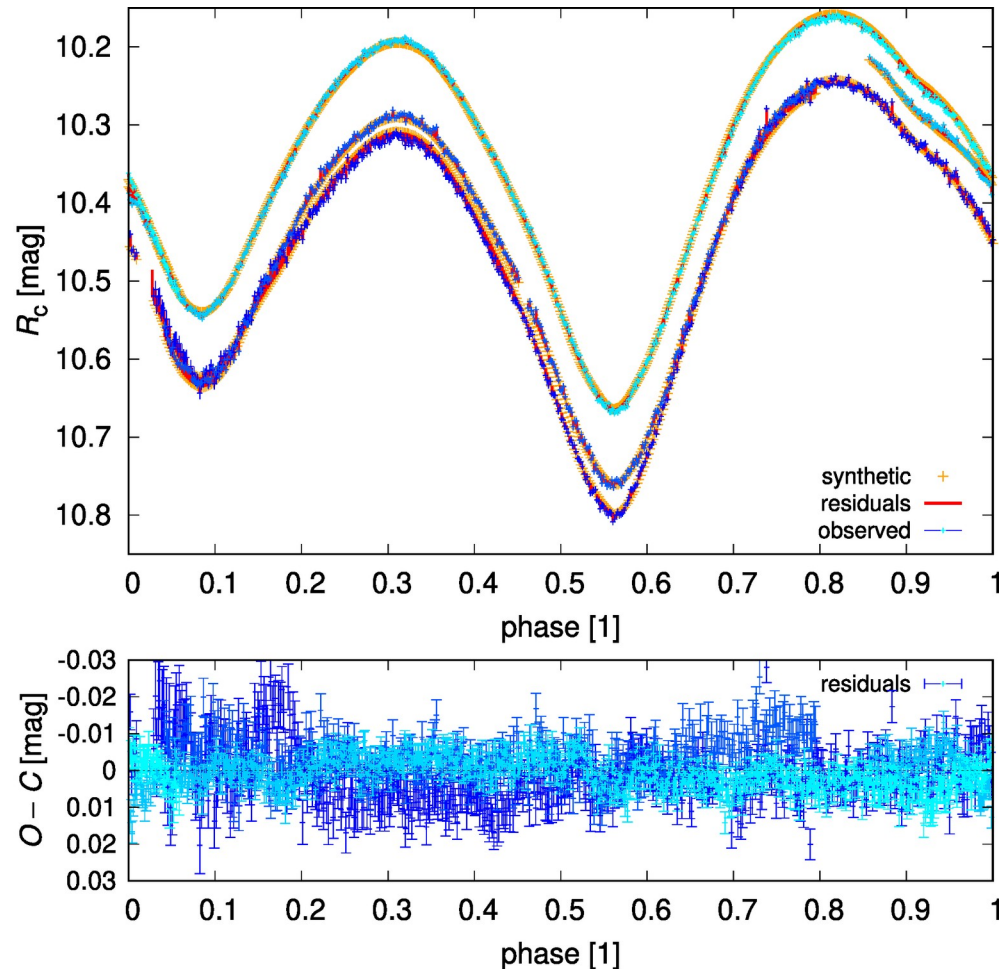


Fig. A.4. Same as Fig. 10, but referring the adjusted shape model of (22) Kalliope. Systematics on the light curves related to the shape were at least partly eliminated. The respective contribution has decreased to $\chi^2_{lc} = 3980$, $n_{lc} = 1829$.

‘Cliptracing’ algorithm

exact synthetic image, pixel = polygon, 3rd clipping: **partial flux-contributions**, no artifacts!

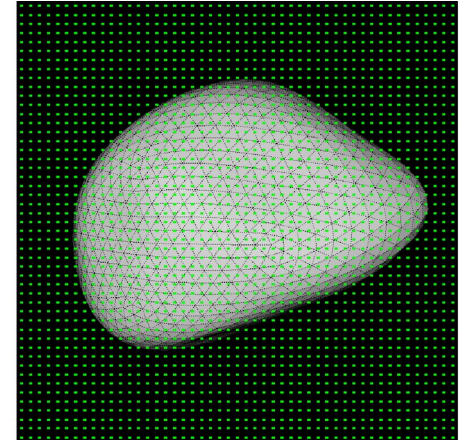
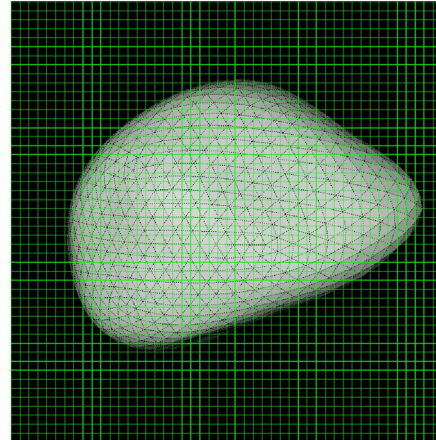
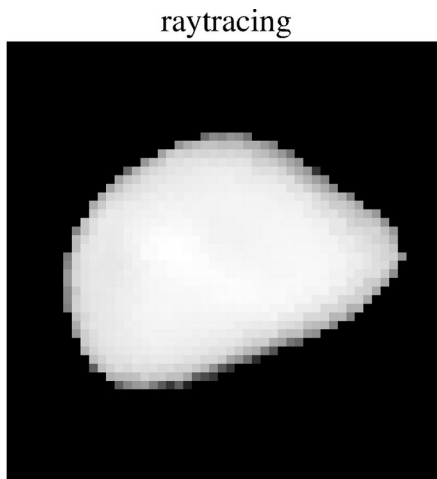
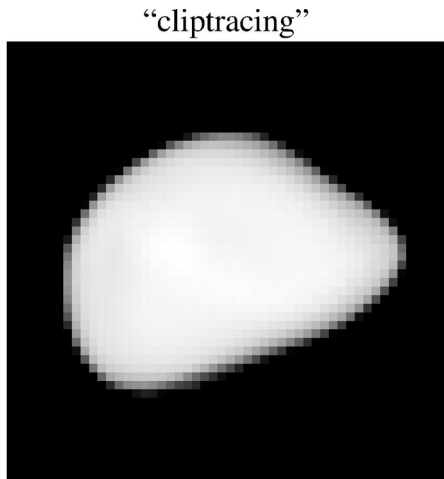


Fig. 4. 1:1 comparison of the ‘cliptracing’ (left) and the raytracing (right) algorithms. In the former, polygons were clipped by individual pixels (analytically) and the synthetic image of (22) is very smooth. In the latter, a simple inside-polygon test was used for each ray, which creates discretisation artefacts and the synthetic image is then ‘noisy’. The Lambert scattering law was used in this test.

Fig. 5. Same as Fig. 4, but showing the corresponding shape composed of polygonal faces (gray) and a grid of either square pixels or points (green).

residuals

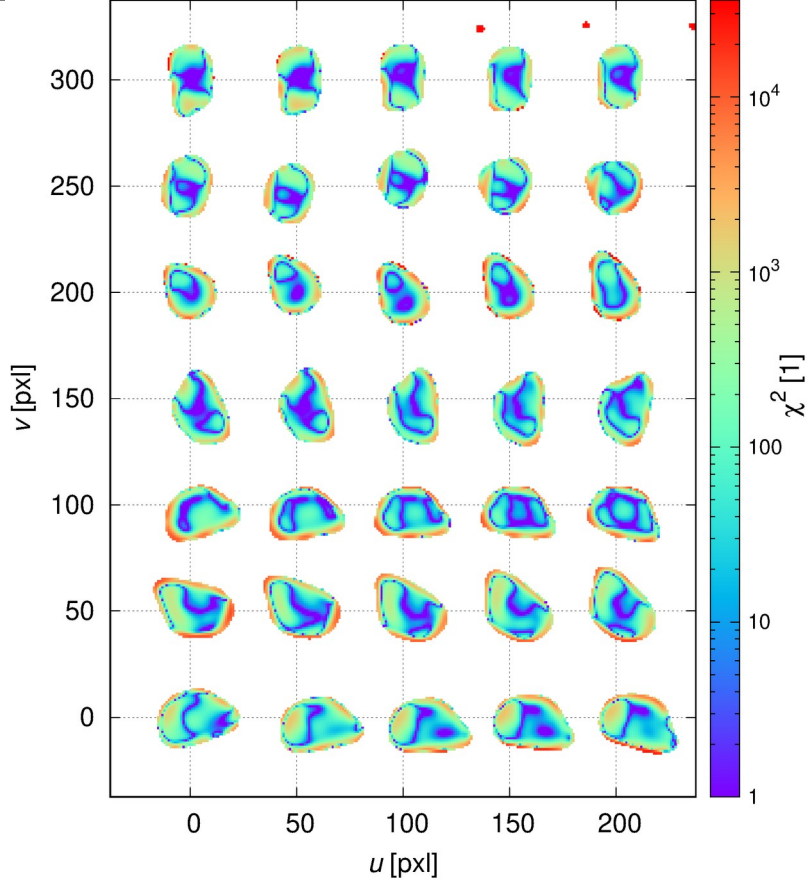


Fig. 17. Residuals from the fitting of 35 deconvolved AO images of (22) Kalliope (taken from Ferrais et al. 2022), with contributions to χ^2 of individual pixels plotted in colour. The projected shape changes due to rotation and viewing geometry. The pixel scale is 3.6 mas pxl^{-1} . After the convergence of the shape parameters, with help of the polygonal algorithm and ‘cliptracing’, the total is $\chi_{\text{ao2}}^2 = 16\,684\,517$, $n_{\text{ao2}} = 22\,843$. Remaining systematics are partly due to rotation, which changes the projected shape during an exposure in a non-trivial way. The observed image of Linus was not fitted (cf. red dots in the upper-right corner).

Future work

- applications of Pyshellspec: φ Per, ω CMa
- improving resolution, AMR?
- synthetic images for multiple * in Xitau
- corr. interferometric observables
- complex orbit + shape fitting
- synthetic spectra for fast-rotating *
- synthetic spectra for pulsating *?
- interferometric module for Phœbe?
- non-LTE radiative transfer in CSM?
- . . .